

# Stabilizer Tensor Networks with Magic State Injection

Azar C. Nakhl,<sup>1,\*</sup> Ben Harper,<sup>1,2,\*</sup> Maxwell West,<sup>1</sup> Neil Dowling,<sup>1,3</sup>  
Martin Sevier,<sup>1</sup> Thomas Quella,<sup>4</sup> and Muhammad Usman<sup>1,2,3</sup>

<sup>1</sup>*School of Physics, The University of Melbourne, Parkville, Victoria 3010, Australia*

<sup>2</sup>*Data61, CSIRO, Clayton, Victoria 3168, Australia*

<sup>3</sup>*School of Physics & Astronomy, Monash University, Clayton, VIC 3800, Australia*

<sup>4</sup>*School of Mathematics and Statistics, The University of Melbourne, Parkville, Victoria 3010, Australia*

(Dated: November 20, 2024)

This work augments the recently introduced Stabilizer Tensor Network (STN) protocol with magic state injection, reporting a new framework with significantly enhanced ability to simulate circuits with an extensive number of non-Clifford operations. Specifically, for random  $T$ -doped  $N$ -qubit Clifford circuits the computational cost of circuits prepared with magic state injection scales as  $\mathcal{O}(\text{poly}(N))$  when the circuit has  $t \lesssim N$   $T$ -gates compared to an exponential scaling for the STN approach, which is demonstrated in systems of up to 200 qubits. In the case of the Hidden Bit Shift circuit, a paradigmatic benchmarking system for extended stabilizer methods with a tunable amount of magic, we report that our magic state injected STN framework can efficiently simulate 4000 qubits and 320  $T$ -gates. These findings provide a promising outlook for the use of this protocol in the classical modelling of quantum circuits that are conventionally difficult to simulate efficiently.

*Introduction.*— Advances in the classical simulation of quantum systems are of utmost importance as they underpin the benchmarking of quantum algorithms [1–6] and enable rigorous tests of nascent claims reporting quantum advantage [7–11]. The state-of-the-art quantum simulation methods primarily revolve around two seemingly independent paradigms: stabilizer methods that can efficiently simulate systems with high entanglement, but struggle with non-Clifford gates [12–14]; or alternatively tensor network-based methods that are well suited to simulations with large number of non-Clifford gates, but scale poorly with entanglement [5, 15, 16]. Therefore, naturally one may seek to amalgamate these methods in such a way as to harness the advantages of both. Indeed, there has been a significant push towards developing such hybrid simulation approaches [17–25], with recent work on the Stabilizer Tensor Network (STN) protocol [25] presenting an efficient technique for the simulation of both highly-magical systems with low entanglement, and highly entangled systems with low magic, loosely defined by the number of non-Clifford operations in the simulation. Building on this, our work demonstrates a marked improvement in the simulability of highly entangled circuits with a large number of  $T$ -gates, achieved by incorporating a tool commonly used in quantum error correction, namely magic state injection [26, 27]. Furthermore, our work provides the first demonstrations of the STN protocol being utilised for benchmarking circuits of interest, namely  $T$ -doped Clifford circuits and the Hidden Bit Shift circuit.

By introducing the use of magic state injection to STNs, we have developed the *Magic state injection Augmented Stabilizer Tensor network* (MAST) simulation framework. To highlight the computational capabilities

of the MAST technique, we benchmark MAST and STN against two commonly used circuits, namely  $T$ -doped Clifford circuits [13, 19, 28, 29] and the Hidden Bit Shift circuit [7, 13, 30–32]. A remarkable finding from our work is that MAST is capable of offering a considerable improvement in simulation cost for some classes of circuits. In particular, for random  $T$ -doped  $N$ -qubit Clifford circuits, MAST is able to efficiently simulate circuits with up to  $N$   $T$ -gates in polynomial time. Beyond this regime, we see a sharp phase transition in simulation cost as the  $T$ -gate density is scaled. Even in this intermediate-depth case, circuits prepared with magic state injection continue to outperform both standard STN and conventional Matrix Product State (MPS) methods until a saturation depth is reached. For the Hidden Bit Shift circuit we find that MAST outperforms STN for relatively few multiply controlled  $Z$  (CCZ) gates. Of note however, is that for both MAST and STN, the bond-dimension appears to scale sub-exponentially, which is in stark contrast to both standard MPS methods and analogous resource costs in stabilizer simulators [7, 13]. Overall, we find that combining STNs with magic state injection is a powerful tool for simulating systems with moderate non-stabilizerness yet high entanglement.

*Stabilizer Tensor Networks.*— The STN protocol [25] is a hybrid simulation method where a quantum state  $|\psi\rangle$  is represented using an MPS in the stabilizer basis as,

$$|\psi\rangle = \sum_{i=1}^{2^N} \nu_i D_i |\phi\rangle \quad (1)$$

where  $\nu_i$  are the coefficients of the basis states,  $|\phi\rangle$  is a stabilizer state as per Appendix A and the  $D_i$  are operators defined with respect to the destabilizer tableau (see Appendix B).

In this protocol, Clifford operations (the gate set generated by  $\{H, S, CNOT\}$  gates) correspond to an update of the basis that can be kept track of in a regular stabi-

\* Contributed Equally

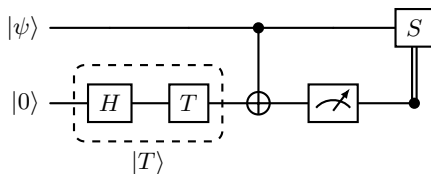


FIG. 1. Magic state injection consists of local operations preparing a magic state, then injection using Clifford gates. If the magic state is measured to be  $|1\rangle$ , a correction gate must be applied. This figure shows the magic state gadget for applying a  $T$ -gate. In this case, the correction is a Clifford gate, but this is not the case in general.

lizer tableau [33], whilst non-Clifford operations can be represented as a sum over elements of the stabilizer basis and correspond to a controlled rotation on the MPS. Expectation values for operators in the stabilizer basis are found using standard MPS methods, which is in general efficient for an MPS in canonical form [15].

An interesting consequence of the set-up of the STN protocol is that non-Clifford operations on un-entangled qubits may be performed in polynomial-time. In contrast, projective measurement, which in tensor-network and stabilizer simulations is computationally efficient, is in fact computationally complex in the STN protocol, corresponding to a sequence of entangling gates on the tensor-network. This can play a significant role in the simulation cost of some classes of circuit.

A more detailed outline of the STN protocol, including how Clifford, non-Clifford and projection operations are performed can be found in Appendix B.

*Magic State Injected Stabilizer Tensor Networks.*— Building on the observation above, we note that in an arbitrary quantum circuit, non-Clifford operations may be replaced by a *state injection gadget*, shown in Figure 1, which uses a pre-prepared magic state and a Clifford injection circuit to apply non-Clifford operations [34]. The protocol finishes with measuring the ancilla magic state qubit and possibly applying a correction, which is a Clifford correction operation for the  $T$  ( $\pi/4$  rotation around  $Z$ ) gate. In a simulator it is possible to predetermine the outcome of this measurement and delay the actual projection until the end of the circuit. We improve STN with the addition of magic state injection, referred to as MAST. When using MAST, magic state preparation and simulation of the resulting Clifford circuit may be performed in polynomial time. The primary cost of a simulation is hence delayed until the final projection step.

It is not immediately obvious that this reframing leads to a computational advantage — in fact, it adds more ancilla qubits and measurements to achieve the same calculation. However, it is thought that the stabilizer tableau in the STN framework stores “potential entanglement” that only transfers to the tensor network when a non-Clifford operation is applied [25]. We posit that an arbitrary circuit may result in an intermediate state with more entanglement than the final state requires [35].

In this case, the projection at the end may be cheaper than applying  $T$ -gates directly. On the other hand, as the cost of simulation scales exponentially with the magic required, the additive computational cost of adding extra ancillas is negligible.

*Results and Discussion.*— To benchmark the effectiveness of both standard and magic state injected STNs, we perform simulations of random  $T$ -doped Clifford circuits as well as the hidden shift circuit. Additionally, to test whether eliminating the cost of the potential entanglement in the stabilizer tableau of the STN protocol is the source of advantage in MAST compared to STN [25], we run the circuit  $U^\dagger U |0\rangle$  for  $U$  generated as a sequence of Clifford +  $T$ -gates as above. While trivial in principle, this computation is in general difficult for standard MPS and stabilizer simulation as a result of the intermediate entanglement and magic generated in the circuit.

*A. Random Circuits.*— We first consider  $T$ -doped Clifford circuits [37] of varying depths, as depicted schematically in Figure 2(a). We define a single layer of such a circuit to consist of a uniformly randomly drawn  $N$ -qubit Clifford operation followed by a  $T$ -gate on the first qubit (the left-right invariance of the uniform measure on the Cliffords combined with the well-known fact that the qubit-permuting operators are Clifford implies that this is equivalent to randomly selecting the  $T$ -gate position at each layer). For depth (number of layers)  $t \gg \log(N)$  this ensemble of random circuits is intractable to simulate using both standard tensor network and stabilizer methods, due respectively to the high entanglement generation of random Cliffords and the exponential-in- $t$  scaling of magic [38, 39], and therefore constitutes an ideal testbed for MAST.

Indeed, we observe stark differences in simulation cost between the different techniques in this setting, finding that MAST significantly outperforms STN. As can be seen in Figure 2(b)-(c) we are able to simulate up to  $N$  layers with bounded average bond dimension using MAST (Region A), in contrast to the exponentially scaling bond dimension displayed by STNs. In the intermediate-depth case of  $N \lesssim t \lesssim 1.5N$  (Region B) we observe a “phase transition”, with the MAST bond dimension increasing exponentially in the number of additional layers. Despite the increase in computational resources required, MAST continues to significantly outperform STNs throughout Region B. Finally, for depths  $t \gtrsim 1.5N$  (Region C), the MAST bond dimension reaches the maximum value of  $2^{N/2}$ .

Now, as is well known, the resources required to simulate an  $N$ -qubit Clifford circuit doped with  $t$   $T$ -gates via the standard stabiliser framework scale as  $\mathcal{O}(\text{poly}(N) \exp(t))$ , and become intractably large when  $t = \mathcal{O}(N)$  [12, 13]. More generally, it is strongly believed that the simulation of Clifford circuits with  $\mathcal{O}(N)$  non-Clifford resources is generically intractable [40]. In this regime, for example, it has been shown that doped Clifford circuits form approximate unitary designs to a precision exponentially small in the system size, repro-

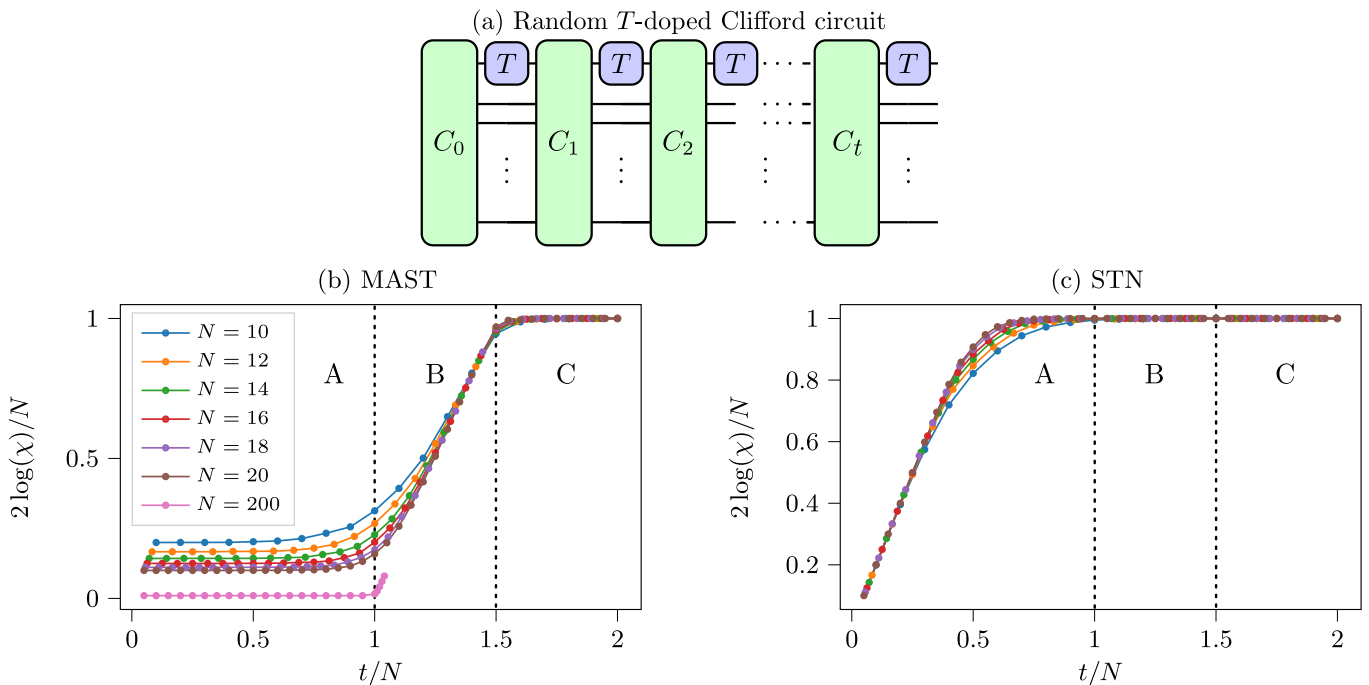


FIG. 2. (a) A schematic illustration of random  $T$ -doped Clifford circuits. The Clifford gates  $C_i$  are generated using the Qiskit SDK [36] using the procedure described in Ref. [37]. (b)-(c) Simulations with the MAST protocol (b) and STN protocol (c) averaged over 1000 random instances. We show the maximum bond-dimension  $\chi$  per MPS required for the complete simulation of a circuit with  $t$   $T$ -gates. Both these axes are scaled with respect to the number of data qubits (i.e. not including the ancilla space for the MAST protocol). We recognise three distinct regions; Region A for  $t \lesssim N$  where MAST has an average bond-dimension bounded by 3 and the bond-dimension for STN exponentially increases with increasing  $t$ ; Region B for  $N \lesssim t \lesssim 1.5N$  where the bond-dimension for MAST exponentially increases with increasing  $t$  and where STN has the maximal bond dimension  $\chi = 2^{N/2}$ ; Region C where both MAST and STN have the maximal bond-dimension of  $\chi = 2^{N/2}$ . We do not simulate more than  $N + 10$  layers for  $N = 200$  due to the exponential increase in bond-dimension.

ducing long-time signatures of quantum chaos [41]. In contrast, we see that MAST is consuming only bounded classical resources up until a critical threshold, which is exactly the expected onset of intractable quantum phenomena. We stress, however, that the MAST protocol does not admit efficient sampling from the probability distributions (in say, the computational basis) characterising these random circuits. While local expectation values may be efficiently computed, projection operations in general cannot. Our results are therefore commensurate with recent works [11, 42] that show the efficient simulability of Pauli expectation values from “locally-scrambling” families of circuits.

In addition to small system sizes of fewer than 20 qubits, we also simulate up to  $t = N + 10$  layers for  $N = 200$  qubits demonstrating that this simulation protocol is scalable. Finally, though not included in Figure 2, we also simulated random circuits with arbitrary  $R_z(\theta)$  rotations replacing the  $T$ -gates, resulting in an identical distribution for the bond-dimension. This is unsurprising, as the different angle only changes the coefficients of the gate decomposition in the STN framework (see Appendix B 2), which ultimately does not influence simulation cost.

Finally, we consider the task of numerically simulating

the trivial circuit  $U^\dagger U |0\rangle$ . We find that for these simulations the bond-dimension is in general significantly greater than 1, indicating that MAST does not universally determine the lowest possible resource cost required for any circuit. We do, however, observe that the resource cost is path dependent where one is free to choose the order in which ancilla qubits are projected. For the particular case of random circuits, projecting pairwise from the middle of the ancilla register out towards either end of that register, one finds that the bond-dimension of the MPS is at most 2 throughout the simulation. This is as a result of each pair of projections generating two CNOT cascades as per Appendix B 4 that cancel each other out such that the result after the pair of projections is a product state. *A priori* one will likely not know the path which minimises the cost of a given simulation. It is an interesting open question to determine a method of finding such an (approximately) optimal projection path.

*B. Hidden Bit Shift.* — We now consider the Hidden Bit Shift circuit [30]. This circuit has two desirable properties for benchmarking; first, it creates a large amount of entanglement, making it difficult to implement for all but stabilizer simulators and fault-tolerant quantum computers, and secondly, a tuneable number of non-Clifford operations, allowing one to easily analyse the performance

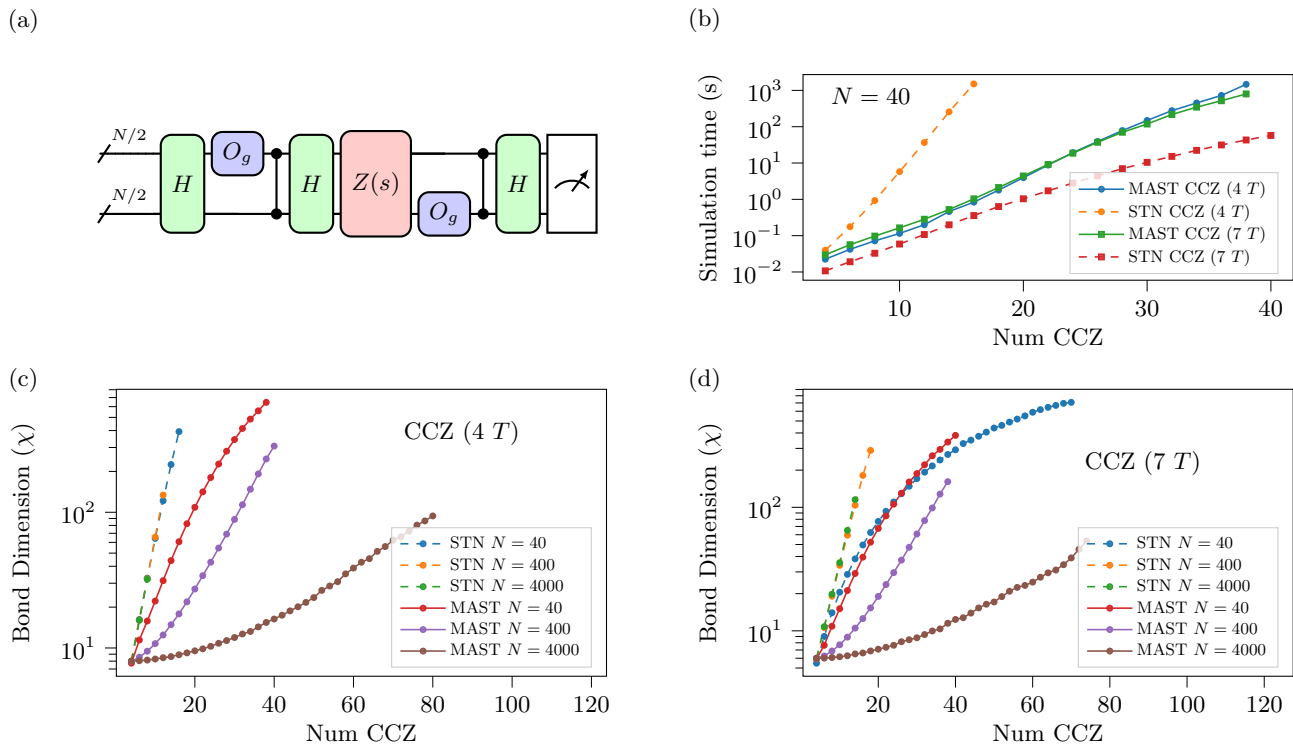


FIG. 3. (a) Hidden Bit Shift Circuit.  $O_g$  is a random phase gate constructed from  $\{Z, CZ, CCZ\}$ .  $Z(s)$  encodes the hidden bit shift, and the final measurement will result in  $s$  with 100% probability. (b) Simulation cost of the hidden-bit shift circuit on 40 qubits. Two cases are simulated, where the CCZ gates are decomposed into four  $T$ -gates + two ancillas, as per [13], and where they are decomposed into seven  $T$ -gates with no extra ancillas. Details of these two decompositions can be found in Appendix C. While conventional STNs are dependent on the decomposition used, MAST is indifferent. (c) Here we simulate the hidden bit shift circuit with much larger numbers of qubits and  $T$ -gates. The number of Clifford operations in  $O_g$  is scaled proportionately with  $N$  to ensure sufficient mixing. The 4  $T$  decomposition is used for these results. As in Figure 2, increasing the number of qubits for a fixed number of  $T$ -gates reduces the simulation cost. (d) Larger simulations using the 7  $T$  decomposition. Simulations were run on Dual 2.45GHz AMD EPYC processors. Each point is an average over 10,000 shots.

of a simulator for different amounts of magic. The class of circuits simulated in this work is identical to that of Refs. [7, 13], and is shown in Figure 3(a).

Compared to Ref. [7], which simulates up to 64  $T$ -gates on 40 qubits using an extended stabilizer simulator that scales exponentially with the number of  $T$ -gates, Figure 3(b) shows that our technique is able to simulate 160  $T$ -gates on 40 qubits. Simulations of the Hidden Bit Shift circuit [7, 13] typically use a four  $T$ -gate decomposition of the  $CCZ$  gate, as these techniques scale only with the number of non-Clifford operations. However, this requires the addition of two ancilla qubits. To explore the effect of this, we also simulated identical Hidden Bit Shift circuits with the standard 7  $T$ -gate decomposition of the Toffoli gate [43]. Details of these can be found in Appendix C. With the 7  $T$ -gate decomposition, the simulation time for STN is lower compared to the 4  $T$ -gate decomposition, while it remains unchanged for MAST despite the circuit containing significantly more  $T$ -gates. These results are explained by the ancilla qubits and extra entangling gates present in the 4  $T$  CCZ, which increase the simulation time for STN.

In Figure 3(c) and (d), we increase the size of the circuits being simulated. As per the results for random  $T$ -doped Clifford circuits, we find that increasing the number of qubits in the Hidden Bit Shift circuit does indeed reduce the bond-dimension under MAST, allowing large circuits of 4000 qubits and 320  $T$ -gates to be simulated on a classical computer. Conversely, STN performs worse at higher qubit counts, and the constant factor advantage of requiring fewer ancillas is drowned out by the exponential cost of magic and entangling gates. Finally, we note that it has recently been shown theoretically that the hidden-shift circuit can be simulated in polynomial-time [44], although this has not been demonstrated in simulation.

*Conclusion and Outlook.*— Exploring the boundaries of the classical simulability of quantum devices is a fundamental task of quantum information theory that has gained increasing practical relevance in the current era of intermediate-scale experimentally-realised quantum computers. Powerful simulation algorithms serve to not only benchmark these devices, but to rigorously test nascent claims of quantum advantage [9, 10]. Indeed,

and in light of this, recent years have seen remarkable progress in the classical simulation of both noisy [42, 45–48] and noiseless [11, 49] quantum computers. Beyond their implied practical advantages, these breakthroughs yield further insight into the nature of quantum computation by identifying with increasing fineness the regimes which are “actually quantum”.

Here, we have extended this body of work by introducing the Magic state injection Augmented Stabilizer Tensor network (MAST) method, and shown it is capable of simulating large circuits that are both highly entangled and magical. We specifically demonstrate this for random  $T$ -doped Clifford circuits, performing simulations with  $\mathcal{O}(N)$   $T$ -gates for up to  $N = 200$  qubits with bounded STN bond dimension. Recently, a similar observation was made for the Clifford Augmented Matrix Product State (CAMPS) protocol [50], which is a different amalgamation of stabilizer and tensor network methods [17, 23, 24] to the STNs considered in this work. Unlike the simulation method devised in this work, the CAMPS-based method requires an optimisation subroutine whereas our method does not.

To further benchmark the utility of MAST, we also considered the Hidden Bit Shift circuit. For this system, we have been able to perform simulations with a significant number of qubits and non-Clifford operations:  $N = 4000$  qubits with 320  $T$ -gates.

The MAST simulation protocol introduced in this work, and stabilizer tensor network methods more broadly have wide reaching applicability and may be used to simulate a variety of quantum algorithms with fewer computational resources than current state-of-the-art simulation protocols. There are many algorithms of interest to the research community with only a moderate amount of entanglement and magic, in particular Noisy Intermediate Scale Quantum (NISQ) [51] algorithms such as the Quantum Approximate Optimisation Algorithm (QAOA) [52], the Variational Quantum Eigensolver (VQE) [53], or Quantum Machine Learning (QML) [2]. Our work may allow larger simulations of

these algorithms using classical resources.

In addition, there is room to further refine MAST and STNs as simulation techniques. As shown in this work, the simulation cost is highly dependent on the decomposition of expensive operations and it may be possible to further optimise these decompositions, similar to the work done optimising magic state decompositions for stabilizer simulators [7, 54]. It may also be possible to replace the tensor network simulator with another simulation method.

Finally, an interesting open question relating to the theoretical underpinning of STN and by extension MAST is how the resource cost of these simulation methods relates to the quantum state that they are simulating, similar to how the bond-dimension of a conventional MPS simulation relates to the entanglement of the state, or how stabilizer rank relates to the magic of the state. This would not only allow for a more direct comparison with other simulation methods where the resource cost is well established but it would also shed a light on precisely what makes certain quantum systems difficult to simulate and narrow down the regime where quantum computers have an advantage over classical computers.

*Acknowledgements.*— A.C.N., M.W., and N.D. acknowledge the support of Australian Government Research Training Program Scholarships. B.H. acknowledges the CSIRO Research Training Program Scholarship. Computational resources were provided by the Pawsey Supercomputing Research Center through the National Computational Merit Allocation Scheme (NCMAS). The research was supported by the University of Melbourne through the establishment of the IBM Quantum Network Hub at the University.

Data Availability: All data generated in this work is presented in figures. Sources and data can be provided upon reasonable request to the corresponding authors.

email: anakhl@student.unimelb.edu.au

email: bharper1@student.unimelb.edu.au

- 
- [1] A. Dang, C. D. Hill, and L. C. L. Hollenberg, Optimising Matrix Product State Simulations of Shor’s Algorithm, *Quantum* **3**, 116 (2019), arXiv:1712.07311 [quant-ph].
  - [2] M. T. West, J. Heredge, M. Sevier, and M. Usman, Provably Trainable Rotationally Equivariant Quantum Machine Learning, *PRX Quantum* **5**, 030320 (2024).
  - [3] M. T. West, S. M. Erfani, C. Leckie, M. Sevier, L. C. L. Hollenberg, and M. Usman, Benchmarking adversarially robust quantum machine learning at scale, *Phys. Rev. Res.* **5**, 023186 (2023).
  - [4] J. Chen, E. Stoudenmire, and S. R. White, Quantum Fourier Transform has Small Entanglement, *PRX Quantum* **4**, 040318 (2023).
  - [5] A. C. Nakhil, T. Quella, and M. Usman, Calibrating the role of entanglement in variational quantum circuits, *Physical Review A* **109**, 032413 (2024).
  - [6] M. Niedermeier, J. L. Lado, and C. Flindt, Simulating the quantum Fourier transform, Grover’s algorithm, and the quantum counting algorithm with limited entanglement using tensor networks, *Physical Review Research* **6**, 033325 (2024).
  - [7] S. Bravyi, D. Browne, P. Calpin, E. Campbell, D. Gosset, and M. Howard, Simulation of quantum circuits by low-rank stabilizer decompositions, *Quantum* **3**, 181 (2019).
  - [8] M. L. Goh, M. Larocca, L. Cincio, M. Cerezo, and F. Sauvage, Lie-algebraic classical simulations for variational quantum computing, *arXiv preprint arXiv:2308.01432* (2023).
  - [9] Y. Kim, A. Eddins, S. Anand, K. X. Wei, E. Van Den Berg, S. Rosenblatt, H. Nayfeh, Y. Wu, M. Zaletel, K. Temme, *et al.*, Evidence for the utility of quantum computing before fault tolerance, *Nature* **618**, 500

- (2023).
- [10] J. Tindall, M. Fishman, E. M. Stoudenmire, and D. Sels, Efficient tensor network simulation of ibm’s eagle kicked ising experiment, *PRX Quantum* **5**, 010308 (2024).
  - [11] A. Angrisani, A. Schmidhuber, M. S. Rudolph, M. Cerezo, Z. Holmes, and H.-Y. Huang, Classically estimating observables of noiseless quantum circuits, *arXiv preprint arXiv:2409.01706* (2024).
  - [12] D. Gottesman, The heisenberg representation of quantum computers, talk at, in *International Conference on Group Theoretic Methods in Physics* (Citeseer, 1998).
  - [13] S. Bravyi and D. Gosset, Improved Classical Simulation of Quantum Circuits Dominated by Clifford Gates, *Phys. Rev. Lett.* **116**, 250501 (2016).
  - [14] C. Gidney, Stim: a fast stabilizer circuit simulator, *Quantum* **5**, 497 (2021).
  - [15] U. Schollwöck, The density-matrix renormalization group in the age of matrix product states, *Annals of physics* **326**, 96 (2011).
  - [16] X. Xu, S. Benjamin, J. Sun, X. Yuan, and P. Zhang, *A Herculean task: Classical simulation of quantum computers* (2023), arXiv:2302.08880 [quant-ph].
  - [17] G. Lami, T. Haug, and J. D. Nardis, *Quantum State Designs with Clifford Enhanced Matrix Product States* (2024), arXiv:2404.18751 [quant-ph].
  - [18] G. Lami and M. Collura, *Learning the stabilizer group of a Matrix Product State* (2024), arXiv:2401.16481 [quant-ph].
  - [19] A. F. Mello, A. Santini, and M. Collura, Hybrid Stabilizer Matrix Product Operator, *Physical Review Letters* **133**, 150604 (2024).
  - [20] X. Qian, J. Huang, and M. Qin, *Clifford Circuits Augmented Time-Dependent Variational Principle* (2024), arXiv:2407.03202 [cond-mat].
  - [21] N. Dowling, P. Kos, and X. Turkeshi, Magic of the Heisenberg Picture, *arXiv preprint arXiv:2408.16047* <https://doi.org/10.48550/arXiv.2408.16047> (2024).
  - [22] A. Paviglianiti, G. Lami, M. Collura, and A. Silva, *Estimating Non-Stabilizerness Dynamics Without Simulating It* (2024), arXiv:2405.06054 [quant-ph].
  - [23] X. Qian, J. Huang, and M. Qin, *Augmenting Density Matrix Renormalization Group with Clifford Circuits* (2024), arXiv:2405.09217 [cond-mat].
  - [24] J. Huang, X. Qian, and M. Qin, *Non-stabilizerness Entanglement Entropy: a measure of hardness in the classical simulation of quantum many-body systems* (2024), arXiv:2409.16895 [quant-ph].
  - [25] S. Masot-Llima and A. Garcia-Saez, *Stabilizer Tensor Networks: universal quantum simulator on a basis of stabilizer states* (2024), arXiv:2403.08724 [quant-ph].
  - [26] S. Bravyi and J. Haah, Magic-state distillation with low overhead, *Physical Review A* **86**, 052329 (2012).
  - [27] A. G. Fowler and C. Gidney, *Low overhead quantum computation using lattice surgery* (2019), arXiv:1808.06709 [quant-ph].
  - [28] S. True and A. Hamma, Transitions in Entanglement Complexity in Random Circuits, *Quantum* **6**, 818 (2022).
  - [29] L. Leone, S. F. E. Oliviero, and A. Hamma, Learning t-doped stabilizer states, *Quantum* **8**, 1361 (2024), arXiv:2305.15398 [quant-ph].
  - [30] M. Roetteler, *Quantum algorithms for highly non-linear Boolean functions* (2009), arXiv:0811.3208 [quant-ph].
  - [31] A. Kissinger, J. v. d. Wetering, and R. Vilmart, Classical simulation of quantum circuits with partial and graphical stabiliser decompositions, *LIPICs, Volume 232, TQC 2022* **232**, 5:1 (2022), arXiv:2202.09202 [quant-ph].
  - [32] A. Kissinger and J. Van De Wetering, Simulating quantum circuits with ZX-calculus reduced stabiliser decompositions, *Quantum Science and Technology* **7**, 044001 (2022).
  - [33] S. Aaronson and D. Gottesman, *Improved Simulation of Stabilizer Circuits* (2008), arXiv:quant-ph/0406196.
  - [34] S. Bravyi and A. Kitaev, Universal quantum computation with ideal Clifford gates and noisy ancillas, *Phys. Rev. A* **71**, 022316 (2005).
  - [35] M. Dupont, N. Didier, M. J. Hodson, J. E. Moore, and M. J. Reagor, Entanglement perspective on the quantum approximate optimization algorithm, *Physical Review A* **106**, 022423 (2022).
  - [36] Qiskit contributors, *Qiskit: An Open-source Framework for Quantum Computing* (2023).
  - [37] S. Bravyi and D. Maslov, Hadamard-free circuits expose the structure of the Clifford group, *IEEE Transactions on Information Theory* **67**, 4546 (2021).
  - [38] S. Aaronson and D. Gottesman, Improved simulation of stabilizer circuits, *Physical Review A* **70**, 052328 (2004).
  - [39] J. Eisert, *Entanglement and tensor network states* (2013), arXiv:1308.3318 [quant-ph].
  - [40] M. J. Bremner, R. Jozsa, and D. J. Shepherd, Classical simulation of commuting quantum computations implies collapse of the polynomial hierarchy, *Proceedings of the Royal Society A: Mathematical, Physical and Engineering Sciences* **467**, 459 (2011).
  - [41] L. Leone, S. F. E. Oliviero, Y. Zhou, and A. Hamma, Quantum Chaos is Quantum, *Quantum* **5**, 453 (2021).
  - [42] A. A. Mele, A. Angrisani, S. Ghosh, S. Khatri, J. Eisert, D. S. França, and Y. Quek, Noise-induced shallow circuits and absence of barren plateaus, *arXiv preprint arXiv:2403.13927* (2024).
  - [43] M. A. Nielsen and I. L. Chuang, *Quantum Computation and Quantum Information* (Cambridge University Press, Cambridge, 2000).
  - [44] M. Amy and L. S. Stinchcombe, *Polynomial-Time Classical Simulation of Hidden Shift Circuits via Confluent Rewriting of Symbolic Sums* (2024), arXiv:2408.02778 [quant-ph].
  - [45] T. Ayril, T. Louvet, Y. Zhou, C. Lambert, E. M. Stoudenmire, and X. Waintal, Density-matrix renormalization group algorithm for simulating quantum circuits with a finite fidelity, *PRX Quantum* **4**, 020304 (2023).
  - [46] D. Aharonov, X. Gao, Z. Landau, Y. Liu, and U. Vazirani, A polynomial-time classical algorithm for noisy random circuit sampling, in *Proceedings of the 55th Annual ACM Symposium on Theory of Computing* (2023) pp. 945–957.
  - [47] E. Fontana, M. S. Rudolph, R. Duncan, I. Rungger, and C. Cirstoiu, Classical simulations of noisy variational quantum circuits, *arXiv preprint arXiv:2306.05400* (2023).
  - [48] G. González-García, J. I. Cirac, and R. Trivedi, Pauli path simulations of noisy quantum circuits beyond average case, *arXiv preprint arXiv:2407.16068* (2024).
  - [49] T. Begušić, K. Hejazi, and G. K. Chan, Simulating quantum circuit expectation values by Clifford perturbation theory, *arXiv preprint arXiv:2306.04797* (2023).
  - [50] G. E. Fux, B. Béri, R. Fazio, and E. Tirrito, *Disentangling unitary dynamics with classically simulable quantum circuits* (2024), arXiv:2410.09001 [quant-ph].

- [51] J. Preskill, Quantum Computing in the NISQ era and beyond, *Quantum* **2**, 79 (2018).
- [52] E. Farhi, J. Goldstone, and S. Gutmann, A Quantum Approximate Optimization Algorithm, *arXiv preprint arXiv:1411.4028* (2014).
- [53] A. Peruzzo, J. McClean, P. Shadbolt, M.-H. Yung, X.-Q. Zhou, P. J. Love, A. Aspuru-Guzik, and J. L. O’Brien, A variational eigenvalue solver on a photonic quantum processor, *Nature Communications* **5**, 1 (2014).
- [54] H. Qassim, H. Pashayan, and D. Gosset, Improved upper bounds on the stabilizer rank of magic states, *Quantum* **5**, 606 (2021).
- [55] D. Gottesman, *Stabilizer Codes and Quantum Error Correction* (California Institute of Technology, 1997).
- [56] R. Orús, A Practical Introduction to Tensor Networks: Matrix Product States and Projected Entangled Pair States, *Annals of Physics* **349**, 117 (2014).

## Appendix A: Stabilizer state and Matrix Product State Background

### 1. Stabilizer states

Stabilizer states  $|\phi\rangle$  are distinguished states that can be completely characterized by specifying an associated stabilizer group  $\mathcal{S}$  [55]. More precisely, the stabilizer group  $\mathcal{S}$  is defined to be the maximal subgroup of the Pauli group  $\mathcal{P}$  over  $N$  qubits such that  $S|\phi\rangle = |\phi\rangle$  for all  $S \in \mathcal{S}$ . From a general theoretical perspective, stabilizers play an important role in error correction as they define a set of operators that are invariant under logical operations [55].

More relevant to our discussion however, is their role in the simulation of circuits consisting only of Clifford gates. Stabilizer states being uniquely defined by their stabilizer group, they can be encoded efficiently in an  $N \times N$  matrix called the stabilizer tableau, where each row is a generator for the stabilizer group. When applying a Clifford gate  $C$  to a stabilizer state, we can find a new set of stabilizers for the updated state by conjugating the stabilizer group  $\mathcal{S}$  by the Clifford operation,

$$\begin{aligned} C|\phi\rangle &= CS|\phi\rangle \\ &= CSC^{-1}(C|\phi\rangle). \end{aligned}$$

When  $C$  is a Clifford gate, conjugating  $S \in \mathcal{S}$  in this way results in a Pauli string [12], which is the updated stabilizer.

Related to the stabilizer group is the destabilizer group  $\mathcal{D} = \mathcal{P}/\mathcal{S}$ , that is the remaining Paulis needed to form the whole group. Although not essential for stabilizer simulators, keeping track of the remaining generators for the Pauli group allows more efficient simulation of projective measurement in a stabilizer simulator [38].

### 2. Matrix Product States

Matrix Product States (MPS) are a tensor network representation of one-dimensional many body quantum systems. For a 2-level system (qubits) whose Hilbert space is spanned by the basis states  $|s\rangle$  where  $s$  is a binary string representation of some number  $1, \dots, 2^N$ , the MPS may be represented as

$$|\psi\rangle = \sum_{s_1, s_2, \dots, s_N} A_{s_1}^{(1)} A_{s_2}^{(2)} \dots A_{s_N}^{(N)} |s_1 s_2 \dots s_N\rangle \quad (\text{A1})$$

where  $A_{s_i}^{(i)}$  are matrices which can be optimally chosen to be of size  $\chi_{i-1} \times \chi_i$ , with the matrices at the end being of size  $1 \times \chi_1$  and  $\chi_N \times 1$  respectively, where  $\chi_i$  is referred to as the bond-dimension (between sites  $i$  and  $i+1$ ) and describes the bipartite entanglement of the state at that site. One may find a lower-entanglement approximation to the state  $|\psi\rangle$  by performing a Singular Value Decomposition (SVD) on the  $A_{s_i}^{(i)}$ , keeping only a fixed number of singular values. A more detailed introduction to MPS may be found in [15].

For simplicity for the upcoming section, we will set  $\nu_i = \text{Tr}(A_{s_1}^{(1)} A_{s_2}^{(2)} \dots A_{s_N}^{(N)})$  where  $i$  is the decimal representation of the binary string  $s_1 s_2 \dots s_N$ . Hence Equation (A1) can be written as

$$|\psi\rangle = \sum_{i=1}^{2^N} \nu_i |i\rangle. \quad (\text{A2})$$

## Appendix B: Stabilizer Tensor Networks

Following the work in [25] that established the Stabilizer Tensor Network (STN) protocol, in this section we describe the foundational aspects of this simulation protocol. Namely we describe how this can be used to describe a general

quantum state, and how it can be used to perform both Clifford and non-Clifford operations, as well as expectation value calculations and projective measurements.

A quantum state  $|\psi\rangle$  in this protocol is represented in the following form,

$$|\psi\rangle = \sum_{i=1}^{2^N} \nu_i D_i |\phi\rangle \quad (\text{B1})$$

where  $|\phi\rangle$  is a stabilizer state stored as a tableau and updated as discussed below, and  $\hat{i} = (s_1, s_2 \dots s_N)$  as above. The operator  $D_i$  is created from the vector  $\hat{i}$ ,

$$D_i = \prod_{j=1}^N \phi_j^{\hat{i}_j} \quad (\text{B2})$$

where  $\phi_j$  is the Pauli string in the  $j^{\text{th}}$  row of  $|\phi\rangle$ 's stabilizer tableau. As  $\mathcal{S} \cup \mathcal{D}$  spans  $\text{End}((\mathbb{C}^2)^{\otimes N})$ , any  $N$  qubit state can be represented in the form of Equation (B1).

### 1. Clifford Operations

To apply a Clifford operation  $C$  to the state  $|\psi\rangle$ , we conjugate the operator  $D_i$  by  $C$

$$\begin{aligned} C |\psi\rangle &= C \sum_i \nu_i D_i |\phi\rangle = \sum_i \nu_i C C^{-1} \tilde{D}_i C |\phi\rangle \\ &= \sum_i \nu_i \tilde{D}_i |\tilde{\phi}\rangle \end{aligned}$$

where  $\tilde{D}_i = C^{-1} D_i C$ . Recall that Clifford conjugation is the update rule for a stabilizer tableau simulator [12], so updating the tableau of  $|\phi\rangle$  is sufficient to update  $D_i$  as well. Hence Clifford operations only update  $|\phi\rangle$ , using the standard stabilizer update rules [38], and leave the MPS unchanged.

### 2. Non-Clifford Operations

To perform a non-Clifford operation  $U$ , first one must find a decomposition of the following form

$$U = \sum_i c_i D_{\hat{d}_i} S_{\hat{s}_i} \quad (\text{B3})$$

where  $c_i$  are complex coefficients, and  $\hat{d}_i$  and  $\hat{s}_i$  are boolean vectors that like  $\hat{i}$  pick out (de)stabilizer rows. These can be found by starting with a decomposition of  $U$  in terms of Pauli strings  $P_i$ ,

$$U = \sum_i a_i P_i, \quad \text{where } P_i = D_{\hat{d}_i} S_{\hat{s}_i}$$

Each  $P_i$  must then be decomposed into products of rows in the (de)stabilizer tableau. We proceed from Proposition 3 in [38], which shows that an element  $(D) S$  in the (de)stabilizer may be written as a product of the (de)stabilizer terms that correspond to rows in the (stabilizer) destabilizer that anticommute with the operator  $(D) S$ . Thus, to find  $D_{\hat{d}_i}$  and  $S_{\hat{s}_i}$  from Equation (B3), we simply check whether  $P_i$  anticommutes with each row in the (de)stabilizer tableau, select the corresponding tableau row, and perform some bookkeeping to keep track of the phase.

After finding the decomposition, one may apply the operator to the STN as follows

$$U |\psi\rangle = \sum_j c_j D_{d_j} S_{s_j} \sum_{i=1}^{2^N} \nu_i D_i |\phi\rangle \quad (\text{B4})$$

$$= \sum_j \sum_{i=1}^{2^N} c_j \nu_i D_{d_j} S_{s_j} D_i |\phi\rangle \quad (\text{B5})$$

$$= \sum_j \sum_{i=1}^{2^N} c_j \nu_i (-1)^{s_j \cdot \hat{i}} D_{d_j + \hat{i}} |\phi\rangle \quad (\text{B6})$$

where we note that the  $i^{\text{th}}$  stabilizer and  $i^{\text{th}}$  destabilizer anti-commute by definition. Also note that  $D_{\hat{j}+\hat{i}} = D_{\hat{j}}D_{\hat{i}}$  for any  $\hat{i}$  and  $\hat{j}$  directly from Equation (B2). We note, that unlike Clifford operations that only update the stabilizer state  $|\phi\rangle$ , non-Clifford operations appear to leave the stabilizer state unchanged, and result instead in an update to the MPS.

Continuing to follow [25], to see how the MPS is updated, consider a decomposition with only two terms  $U = c_1 D_{\hat{d}_1} S_{\hat{s}_1} + c_2 D_{\hat{d}_2} S_{\hat{s}_2}$ . We can write this as

$$U = (c_1 I + c_2 D_{\hat{d}_2} S_{\hat{s}_2} S_{\hat{s}_1} D_{\hat{d}_1}) D_{\hat{d}_1} S_{\hat{s}_1} \quad (\text{B7})$$

recognising that  $S_{\hat{i}} S_{\hat{i}} = D_{\hat{i}} D_{\hat{i}} = I$  for any boolean vector  $\hat{i}$ . We note that the  $D_{\hat{d}_1} S_{\hat{s}_1}$  on the right hand side simply correspond to Clifford gates on all  $\hat{i}$  qubits. The remaining operation  $\tilde{U} = (c_1 I + c_2 D_{\hat{d}_2} S_{\hat{s}_2} S_{\hat{s}_1} D_{\hat{d}_1})$  can then be written as a multi-qubit rotation operation

$$\tilde{U} = \cos(\theta) I + e^{i\alpha} \sin(\theta) D_{\hat{d}_2} S_{\hat{s}_2} S_{\hat{s}_1} D_{\hat{d}_1} \quad (\text{B8})$$

$$= \cos(\theta) I + e^{i\alpha} (-1)^{\hat{d}_2 \cdot (\hat{s}_1 + \hat{s}_2)} \sin(\theta) D_{\hat{d}_2} D_{\hat{d}_1} S_{\hat{s}_2} S_{\hat{s}_1} \quad (\text{B9})$$

where one can find that  $c_1 = \cos(\theta)$  and  $c_2 = e^{i\alpha} \sin(\theta)$  by computing  $U U^\dagger$  from Equation (B3) (see Annex A, Lemma 2 of [25]) and where we utilise the (de)stabilizer commutation relation. One can readily see that this is of the form of a multi-qubit rotation operation over the qubits  $\hat{s}_1 + \hat{s}_2$  and  $\hat{d}_1 + \hat{d}_2$ .

For multi-qubit operators that have more than two terms in their decomposition, one may recursively apply the above procedure between the 1<sup>st</sup> to 2.. $i^{\text{th}}$  elements of the decomposition to determine a nested sequence of controlled rotations. However given that one typically constructs multi qubit operations given a basis of Cliffords operators and arbitrary  $Z$  rotations, which only require two terms in their decomposition, we do not further consider multi-qubit non-Clifford operations.

### 3. Expectation Values

To determine expectation values of some operator  $O$  one must determine the decomposition in the form of Equation (B3), noting that for Pauli expectation values this can always be done with a single term, i.e.  $O = \alpha D_{\hat{a}} S_{\hat{b}}$ . Given this one can find the expectation value on the MPS directly by first applying  $Z$  ( $X$ ) gates that result from the  $D_{\hat{a}}$  ( $S_{\hat{b}}$ ) then following the standard prescription for computing expectation values [56]. We note that provided that the MPS is in canonical form, the computation of local expectation values may be performed in polynomial time.

### 4. Projection

Given an expectation value, as determined above, one may perform a projective measurement by performing the computation  $\frac{1+pO}{2} |\psi\rangle$  where  $p$  is the measurement outcome selected based off  $\langle O \rangle$ . This results in the following outcome,

$$\frac{1+pO}{2} |\psi\rangle = \frac{1}{2} \sum_{i=1}^{2^N} c_i (D_{\hat{i}} + \alpha p (-1)^{\hat{a} \cdot \hat{i}} D_{\hat{i} \cdot \hat{b}}) |\phi\rangle. \quad (\text{B10})$$

This may be performed using the following operation on the MPS

$$\text{Proj}_p = |0\rangle\langle 0|_k \frac{1}{\sqrt{2}} I \pm \frac{\alpha (-i)^{\hat{a} \cdot \hat{b}}}{\sqrt{2}} D_{\hat{a}} D_{\hat{b}} \quad (\text{B11})$$

where  $k$  corresponds to the first destabilizer row that anti-commutes with  $O$ . One must then perform the projective measurement on the stabilizer tableau by following the standard formalism as outlined in [38] and re-normalise the MPS.

An alternative way to view projection is purely via the stabilizer tableau, where we note that the procedure to update the stabilizer tableau results in the multiplication of (de)stabilizer rows that anti-commute with the operator, which is precisely what is occurring in Equation (B10). The tableau update procedure also results in the projection of the first destabilizer row that anti-commutes with  $O$ , which again directly corresponds to what is occurring in the MPS.

An interesting observation to make here, and one that is pertinent in this work is that projection is a computationally complex operation as the operator in Equation (B11) is an operation akin to a controlled rotation, similar to that in Equation (B9) for non-Clifford operations.

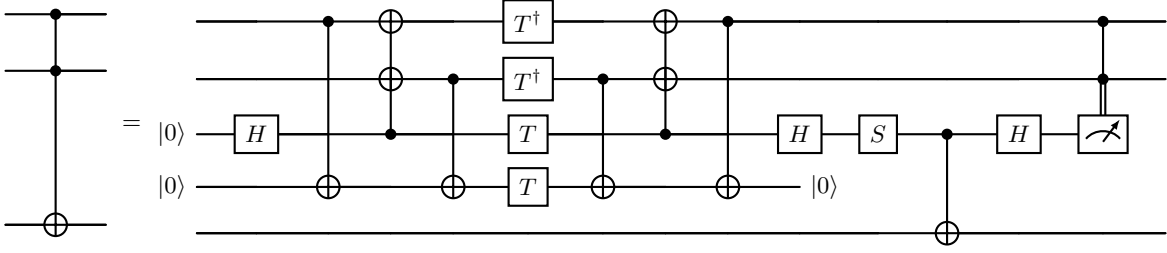


FIG. 4. A Toffoli gate ( $CCX$ ) decomposition as per Ref. [13] with 4 non-Clifford operations ( $T, T^\dagger$ ) and 8 two-qubit Clifford operations. This decomposition requires 2 ancillary qubits, one of which may be reused. This may be turned into a decomposition for  $CCZ$  by application of  $H$  gates at the start and end of the target register.

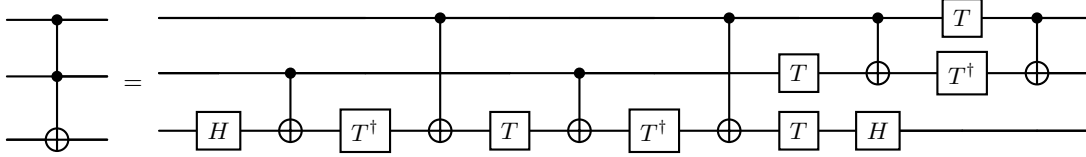


FIG. 5. A standard Toffoli gate ( $CCX$ ) decomposition [43] with 7 non-Clifford operations ( $T, T^\dagger$ ) and 6 two-qubit Clifford operations. Note like Figure 4, one may turn this decomposition into one for the  $CCZ$  gate by application of two  $H$  gates.

### Appendix C: $CCZ$ Gate Decompositions

The main body of this work utilised the decomposition of the  $CCZ$  gate used in Ref. [7, 13] as shown in Figure 4. The primary motivation for this decomposition is to minimise the number of non-Clifford operations required as that is the expensive resource for stabilizer simulators. The trade-off here is that this decomposition requires ancilla qubits, and additionally requires more entangling gates compared to the standard decomposition as shown in Figure 5. Hence the decomposition in Figure 4 is suited to simulation methods constrained by magic, whereas the decomposition in Figure 5 is well suited to simulation methods constrained by entanglement.